Mutation Research 736 (2012) 48–55

Contents lists available at ScienceDirect

Mutation Research/Fundamental and Molecular Mechanisms of Mutagenesis

journal homepage: www.elsevier.com/locate/molmut
Community address: www.elsevier.com/locate/mutres

Aging and photo-aging DNA repair phenotype of skin cells—Evidence toward an effect of chronic sun-exposure

Chloé Prunier[a], Gwénaëlle Masson-Genteuil[a], Nicolas Ugolin[b], Fanny Sarrazy[a], Sylvie Sauvaigo[a,*]

[a] Laboratoire Lésions des Acides Nucléiques, CEA, DSM, INAC, SCIB, UMR-E CEA/UJF-Grenoble 1, 17 Rue des Martyrs, F-38054 Grenoble Cedex 9, France
[b] Laboratoire de Cancérologie Expérimentale, CEA, DSV, IRCM, SREIT, BP6, Fontenay-aux-Roses Cedex F-92265, France

ARTICLE INFO

Article history:
Received 25 October 2010
Received in revised form 18 April 2011
Accepted 7 May 2011
Available online 2 June 2011

Keywords:
DNA repair assay
Biochip
Fibroblasts
UVB irradiation
Aging

ABSTRACT

Several studies have demonstrated the deleterious effect of aging on the capacity of cells to repair their DNA. However, current existing assays aimed at measuring DNA repair address only a specific repair step dedicated to the correction of a specific DNA lesion type. Consequently they provide no information regarding the repair pathways that handle other types of lesions. In addition to aging, consequences of photo-exposure on these repair processes remain elusive. In this study we evaluated the consequence of aging and of chronic and/or acute photo-exposure on DNA repair in human skin fibroblasts using a multiplexed approach, which provided detailed information on several repair pathways at the same time. The resulting data were analyzed with adapted statistics/bioinformatics tools. We showed that, irrespective of the repair pathway considered, excision/synthesis was less efficient in non-exposed cells from elderly compared to cells from young adults and that photo-exposure disrupted this very clear pattern. Moreover, it was evidenced that chronic sun-exposure induced changes in DNA repair properties. Finally, the identification of a specific signature at the level of the NER pathway in cells repeatedly exposed to sun revealed a cumulative effect of UVB exposure and chronic sun irradiation. The uses of bioinformatics tools in this study was essential to fully take advantage of the large sum of data obtained with our multiplexed DNA repair assay and unravel the effects of environmental exposure on DNA repair pathways.

1. Introduction

Aging in humans is a complex, multifactorial process and it is generally admitted that two distinct components play a decisive role in its evolution: one linked to the genetic background of the individuals and one related to their lifestyle and history of exposure to environmental and endogenous mutagens [1]. Cellular functions have been shown to decline with aging [2] and DNA repair mechanisms, as part of a general biological process, are subjected to age-dependent changes [1,3]. Several studies have demonstrated that aging is accompanied by an increase in persistent DNA lesions and mutations in genomic DNA [3–5], and as a consequence, accumulation of somatic damages. Age-related modifications of DNA repair enzyme activity as well as changes in repair enzyme expression and subcellular distributions could be partly responsible for these nuclear and mitochondrial genomic defects [6]. In addition, the cellular stress-response systems such as the reactive oxygen species (ROS) signalling pathways and antioxidant defences [7–9] are modified with aging and contribute to the acceleration of this process. Hence, the DNA repair capacities of individuals reflect their initial genetic genome maintenance properties modulated by the somatic modifications driven by endogenous/exogenous chemicals encountered by cells during the life time.

Skin offers an interesting model to investigate these issues and discriminate between the contribution of endogenous stress and chronological aging on the one hand, and the additional consequences of the exposure of skin cells to the genotoxic sun ultra-violet (UV) radiations, on the other hand. As a matter of fact, in contrast to cells from photo-protected zones, cells from photo-exposed skin areas might have accumulated additional specific UV-driven changes responsible for drastic consequences illustrated for example by the increasing incidence of skin cancers [10]. Consequently, the determination of DNA repair capacities of adequate representative skin samples should be informative on the effects of these distinct endogenous and exogenous factors.

Abbreviations: AbaS, abasic sites; AlkB, alkylated bases; BER, base excision repair; CisP, cisplatine; CPD-64, cyclobutane pyrimidine dimer and 6–4 photoproduct; CTRL, control; FI, fluorescence intensity; MAD, median absolute deviation; MeV, multiexperiment viewer; NER, nucleotide excision repair; 8oxoG, 8-oxo-7,8-dihydroguanine; PCA, principal component analysis; PE, photo-exposed; PP, photo-protected; ROS, reactive oxygen species; TFI, total fluorescence intensity; UVB, ultra-violet B.

* Corresponding author. Tel.: +33 4 38 78 37 52; fax: +33 4 38 78 50 90.
E-mail address: sylvie.sauvaigo@cea.fr (S. Sauvaigo).

0027-5107/$ – see front matter © 2011 Elsevier B.V. All rights reserved.
doi:10.1016/j.mrfmmm.2011.05.005

Recent studies from our group and others converge toward an age-related reduction in the nuclear DNA repair capacity in mammalian cells and tissues [11–16]. However, in apparent contradiction with these findings, we also found that, in contrast to what happens for the excision of most modifications by base excision repair (BER), the excision rate of 8oxoG increased with aging in skin cells [15], whereas excision/synthesis repair globally declined [17]. These findings raised some interesting questions about the possible adaptation of certain enzymes to the age-associated oxidative environment.

Numerous studies showed that repeated UV exposure causes extrinsic aging of skin-called photo-aging – characterized by the early appearance of hallmarks of natural aging [18] that reflect the functional decline of cell regulation pathways. However, in recent studies we found no effect of chronic sun exposure either on excision/synthesis or on BER activities when comparing chronically photo-exposed (PE) and photo-protected (PP) fibroblast extracts from the same donors in a cohort of volunteers of different ages [12,17]. To our knowledge, up to now, no direct demonstration of chronic skin UV exposure as a contributing factor in the deregulation of DNA repair systems in skin cells has been provided.

In order to gain further insights into the possible consequences of cumulative effects of aging and photo-exposure on DNA repair systems, we therefore decided to investigate the repair response of PP and PE fibroblasts exposed to an additional acute UV challenge applied *in vitro* as a function of age of the donors. We thus examined excision/synthesis capacities of cultured primary fibroblasts 24 h after a moderate UVB irradiation as a function of donor age and initial skin biopsy status (PP or PE) using an *in vitro* multiplexed functional assay. This strategy was chosen as this UVB dose was previously shown to trigger a DNA repair response, 24 h after irradiation, in repair-proficient human fibroblasts contrary to what happened in repair-deficient cells [19].

We used analysis/classification methods developed for microarray approaches to analyze the data obtained in our multiplexed assay and address the impact of UV exposure on the DNA repair capacities in the different groups of skin cells. These powerful analysis methods allowed the extraction of relevant information from complex data and revealed the specific contribution of intrinsic aging and UV-irradiation (exogenous genotoxic attack) to functional DNA repair changes.

2. Material and methods

2.1. Cell culture and irradiation

We used the fibroblast library previously established as described from skin biopsies of thirty female volunteers of different ages [12,17]. Biopsies were obtained in accordance with ethical procedures (Helsinki Guidelines) after approval by a Medical Ethics Committee (CCPPRB). Briefly, two 3 mm punches were taken for each volunteer: one on dorsal forearm (photo-exposed area) and one on the volar forearm (photo-protected area). The fibroblast cultures were established by outgrowth of the punches previously cut into small pieces. For each donor, two different cell cultures were established: one from a photo-protected area and one from a photo-exposed area. Cells were cultured in M199 medium (Invitrogen, Cergy-Pontoise, France) supplemented with 10% FCS and containing 100 U/mL penicillin and 100 μg/mL streptomicin at 37 °C in a 5% CO_2 humidified atmosphere. For UVB irradiation, the cells (called I) were plated in 100 mm petri dishes at passage 8. Twenty four hours after seeding, the culture medium was replaced by PBS and the cells irradiated. The PBS was then replaced by the preserved medium and the cells were cultured for an extra 24 h. Cells were harvested at 70–80% confluence and stored frozen in liquid nitrogen in culture medium containing 10% DMSO ($2–3 \times 10^6$ cells per pellet). The irradiance received by the samples was 0.2 W/m^2 corresponding to an irradiation of 25 s at a dose of 5 J/m^2 delivered by a VL 215G irradiator emitting at a wavelength centred around 312 nm (TL-12 Philips lamp, Bioblock Scientific, Illkirch, France; spectrum shown in Supplemental data, Fig. A). It was monitored using a VLX 3 W radiometer (Vilbert Lourmat, Marnes la Vallée, France) equipped with a 312 nm probe. This irradiation condition was chosen as we showed that it induces DNA repair activities in repair-proficient human fibroblasts with very little cell mortality [19]. Mock treated cells (called C) were processed the same way except for the irradiation. For each donor, we ended up with 4 cell pellets (PPC, PEC, PPI, and PEI).

Three Age Groups (AG) were constituted: AG1: 20–33 years old (mean age = 25 years), AG2: 40–50 years old (mean age = 46 years), AG3: 61–68 years old (mean age = 65 years). About 8–10 samples were available per age/exposure group.

2.2. Cell nuclear extracts

Nuclear extracts were prepared as described [19]. Briefly, thawed cells were washed twice in ice-cold PBS, suspended in 1 mL of ice-cold buffer A (10 mM HEPES pH 7.9, 1.5 mM $MgCl_2$, 10 mM KCl, 0.01% Triton X-100, 0.5 mM DTT, and 0.5 mM PMSF) and left on ice for 20 min. The tubes were vortexed for 30 sec to achieve complete cytosol membrane lysis. The nuclei were recovered by centrifugation 5 min at 5000 rpm at 4 °C. They were then suspended in 25 μL of ice-cold buffer B (10 mM HEPES pH 7.9, 1.5 mM $MgCl_2$, 400 mM KCl, 0.2 mM EDTA, 25% glycerol, 0.5 mM DTT, antiproteases (Complete-mini, Roche, Meylan, France) and 0.5 mM PMSF (phenylmethylsulfonyl fluoride)). Nuclear membranes were lysed for 20 min on ice, and two cycles of freezing–thawing at −80 °C and 4 °C respectively. The extracts were centrifuged for 10 min at 13,000 rpm at 4 °C. The supernatant was recovered and stored frozen in 10 μL aliquots at −80 °C. Protein content was determined using the BCA kit (Interchim, Montluçon, France). Typical protein content was around 1 mg/mL.

2.3. Preparation of the damaged plasmid biochips

The damaged plasmid biochips were prepared as described [19] except that the hydrogel slides were prepared in our laboratory. Twelve slides were prepared simultaneously. Before casting the gel, the slides were pre-treated with Bind Silane (γ-methacryloxypropyltrimethoxysilane, GE Healthcare, Orsay, France). We then prepared deoxygenated Hydrogel Solution A (1 mL) from BMT Biosystem (Woodbridge, CT, USA) to which was added 10 μL of a 1/10 diluted solution of TEMED (N,N,N′,N′-tetramethylethylenediamine) and 10 μL ammonium persulfate 10% (w/v) (both from Sigma, St. Louis, MO, USA). The slides were set onto a glass plate pre-treated with dimethyldichlorosilane (Sigma, St. Louis, MO, USA) with tape as spacer. The gel solution was layered on the top of the plate and covered with the slides (100 μL per glass slide). After 2 h, the slides were disassembled from the plate, rinsed 2×5 min in H_2O, dried for 5 min at 30 °C and stored at 4 °C until spotting.

In the present study we used 6 categories of damaged plasmids containing the following lesions: photoproducts (cyclobutane pyrimidine dimers and (6–4) photoproducts; CPD-64 plasmid) generated by UVC irradiation, 8-oxoguanine (8oxoG plasmid) generated by riboflavin photosensitization, alkylated bases (AlkB plasmid) obtained by treatment of the plasmid with *trans*, *trans*-2-4-decadienal (Sigma, St. Louis, MO, USA), cisplatin adducts (CisP plasmid) obtained by incubation of the plasmid DNA with cisplatin in DMSO, abasic sites (AP sites; AbaS plasmid) created by acidic treatment (pH 4.8) of the plasmid DNA, and cytosine and thymine glycols (glycol plasmid) formed by treatment of the plasmid with $KMnO_4$ (Sigma, St. Louis, MO, USA). Before spotting, each type of modified plasmid was diluted in non modified plasmid to generate 3 different solutions of identical DNA concentration (40 μg/mL) but with 3 different ratios lesion/DNA (ratios ½, ¾ and 1, called A, B and C dilutions, respectively). Lesion quantification on plasmid DNA has been published elsewhere [19] (see Supplemental data, Table A). Each spot was duplicated. Nine spots of Control plasmid (CTRL; plasmid without any modification) were deposited on each biochip together with the damaged plasmids. Twelve identical pads (i.e.12 biochips) were prepared per slide.

2.4. Excision/synthesis reaction

The excision/synthesis reactions were conducted for 3 h at 30 °C. Reaction chambers (Grace Bio-Labs, Bend, OR, USA) were set on the damaged plasmid microarray slides and filled with 20 μL of the repair mix containing 5 μL of 5× ATG buffer (200 mM Hepes KOH pH 7.8, 35 mM $MgCl_2$, 2.5 mM DTT, 1.25 μM dATP, 1.25 μM dTTP, 1.25 μM dGTP, 17% glycerol, 50 mM phosphocreatine (Sigma, St. Louis, MO, USA), 10 mM EDTA, 250 μg/mL creatine phosphokinase, 0.5 mg/mL BSA), 1 mM ATP (Amersham, Little Chalfont, England), 1.25 μM dCTP-Cy5 (Amersham, Little Chalfont, England), and extracts at a final protein concentration of 0.15 mg/mL. Then the slides were washed for 2×3 min in PBS/Tween 0.05%, and for 2×3 min in MilliQ water. The slides were then centrifuged 3 min at 700 rpm, and dried 5 min at 30 °C in an incubator.

The samples with a protein concentration too low for being tested at 0.15 mg/mL were eliminated. The remaining 104 samples (out of 124) were tested in duplicate on two different slides.

To allow correction for any potential inter-experimental variability, two repair reactions performed on two different slides were conducted per experimental day using commercial HeLa nuclear extracts (CilBiotech, Mons, Belgium), kept frozen in aliquots at −80 °C. The HeLa extracts were used at a final protein concentration of 0.20 mg/mL.

2.5. Microarray scanning, fluorescence quantification

Images were acquired at 635 nm wavelength at 5 μm resolution using a Genepix 4200A scanner (Axon Instrument) with a Gain of 520. Total spot Fluorescence Intensity was determined using the Genepix Pro 5.1 software (Axon Instrument).

2.6. Data normalization

Results could present an inter-experiment variation attributed mainly to the Cy5 label, which was sensitive to ozone conditions. A daily corrective factor was thus calculated using the data from HeLa extract experiments. More precisely, a first normalization was performed on duplicated HeLa results obtained each day, using the NormalizeIt software already described [19]. Then the set of normalized HeLa data for one day was selected as a reference. Intensities of each HeLa normalized dataset for other days were plotted against intensities of the reference HeLa dataset, to generate a scatter graph. A linear regression fit was generated using this scatter graph and the slope extracted from this regression was used to correct the results obtained each day.

The data of each sample duplicate were also normalized with the NormalizeIt software.

2.7. Data treatment

The total fluorescence incorporated during the repair of each lesion (fluorescence intensity, FI) was calculated by adding the fluorescence of the corresponding A, B and C plasmid dilutions. For consistency with regard to the 3 lesion dilutions that were added, the value used for the control plasmid was the fluorescence intensity of the Control multiplied by 3 (called CTRL).

Each sample was thus characterized by 7 values: the FI obtained for each of the 6 lesions and for the CTRL, which represents non specific excision/synthesis activities. To simplify the analysis, we considered that these 7 values represented distinct "lesions" and the excision/synthesis repair capacity of a sample was determined as being the total fluorescence intensity (TFI) calculated by adding the corresponding seven FI.

2.8. Statistical approaches

2.8.1. Standardization of the data

Data were standardized using the median absolute deviation (MAD) so that for each lesion, fluorescence intensity of all samples had a median of zero and a MAD of 1. As the average FI obtained for the different lesions have different levels and dynamic range, this robust standardization method is the most convenient way to appreciate simultaneously all results (see Section 2.8.3).

2.8.2. Principal component analysis (PCA)

The PCA analyses were constructed with the software "R" [20]. For this analysis, each lesion, including the CTRL, was considered. Principal component analysis (PCA) is applied frequently to explore multidimensional data in a low-dimensional space. It gives an overview of complex data using small number of principal components [21]. Here, the different lesions (and consequently DNA repair processes) were described with the so called principal components, in order to assess relations between them. Correlations between the different lesions were then visualized on the correlation circle. PCA was applied on standardized data (Fig. 1).

To confirm the results obtained with the PCA, we ran Spearman correlation tests. This method, compared to Pearson correlation, limited the weight of outliers. All statistical tests were run using R.

2.8.3. Descriptive statistics

Standardized FI data are displayed as box plots to compare the distribution between the 12 different groups defined according to Age Groups (1, 2 and 3) and exposure status (PPC, PEC, PPI, and PEI) (Fig. 2).

Differences between groups were evaluated for all lesions on all the possible couples between the 12 groups using non parametric tests. To determine the effect of age within groups of identical exposure status, the Wilcoxon signed-rank test for two independent groups was chosen. For each test (each lesion), two one-sided alternative hypotheses were tested to verify if the difference between the medians of 2 groups was greater or less than zero. Results of the statistical analysis are reported in Table 1.

2.8.4. Hierarchical clustering

For this analysis, we used the web-available algorithm of the TIGR MultiExperiment Viewer (MeV) software (http://www.tm4.org/mev.html). To compare the repair phenotype of the different samples, the CTRL FI was considered as the internal reference for each sample; each lesion FI for a given sample was divided by the corresponding CTRL FI. Thus, following this normalization, the repair level of the different categories of lesions was expressed as the "signal fold increase over the CTRL". For the hierarchical clustering representation, the logs of these ratios were used to symmetrise their distribution around zero.

Hierarchical clustering was initially performed on the whole dataset (Fig. 3). The data were subsequently organized into a series of six matrix NPs where the lines N represented the samples (individuals) and the columns P represented the lesions (CPD-64, 8oxoG, AlkB, CisP, AbaS and glycol) for each condition. Each exposure couple PPC/PPI, PPC/PEI, PPC/PEC, PEC/PPI, PEC/PEI, PPI/PEI, was represented in one matrix. A two-way ascending hierarchical classification was then performed, firstly on the lines (individuals) and secondly on the columns (lesion type according to exposure) of the six matrix [22]. This clustering strategy firstly groups together individuals according to their repair patterns, revealing the contribution of age. Secondly, it classifies the lesion types associated with exposure status using the whole population of individuals, revealing the relationship among repair pathways. This relationship is then represented by a tree whose branch lengths reflect the degree of dissimilarity between the repair responses.

The clustering method was combined with a graphical display, each cell (or data point) being represented by a colour that quantitatively reflected the experimental result. Cells with log ratios of 0 (ratio of 1.0, CTRL FI = lesion FI) were coloured black, increasingly positive log ratios with reds of increasing intensities, and inversely, increasingly negative log ratios with greens of increasing intensity. The end product (colour map) allowed a visualization of the relationships between repair pathways and exposure groups (Figs. 4–6).

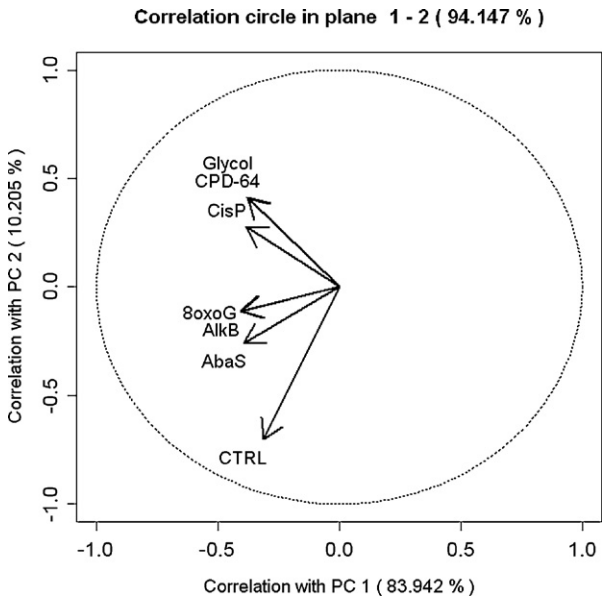

Fig. 1. Correlation circle of a principal component analysis performed on the interactions between what were considered as different DNA repair pathways. The whole dataset was used for this analysis (standardized data). Each arrow represented the repair of a given lesion. The present plane explained 94.15% of the variance within the dataset. Neighbouring arrows reflected strong correlations between repair pathways. The correlations were subsequently confirmed by a Spearman correlation test (see Supplemental data, Fig. B).

3. Results and discussion

3.1. Consideration about the samples

The consequences of *in vitro* aging, related to the number of cell passages in culture, are hardly addressed in the literature. Kaneko et al. found an accumulation of 8oxoG content in DNA during *in vitro*

Table 1
Effect of age (by Age Group) within each exposure group on the different DNA repair activities (fluorescence intensity corresponding to each lesion). To determine the effect of age, the Wilcoxon signed-rank test for two independent groups was run. For each test, two one-sided alternative hypothesis were tested to verify if the difference was greater or less than zero (> or <). See Fig. 2 for related box-plots.

Exposure status	Lesions	Comparison between Age Groups
PPC	8oxoG,* AbaS,* AlkB,** CPD-64,* CisP,* glycol*	1 > 2
	AlkB,** CPD-64,* glycol*	1 > 3
	AlkB*	2 < 3
PEC	Glycol*	1 > 3
PEI	Glycol*	1 > 2
	Glycol*, CisP*	1 > 3

* Only the significant differences between groups are reported ($p < 0.05$).
** Only the significant differences between groups are reported ($p < 0.01$).

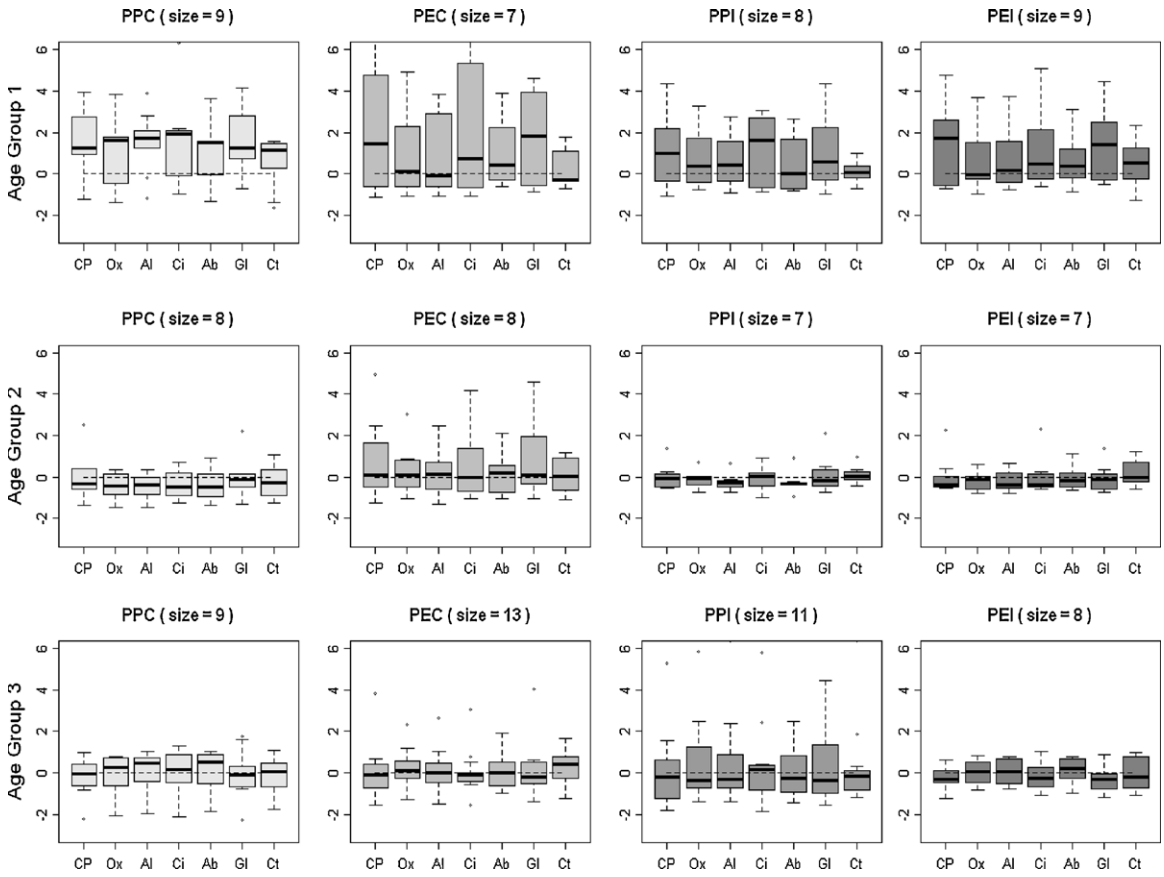

Fig. 2. Box plots displaying the standardized fluorescence intensity (FI) for each lesion and the CTRL sorted by Age Group (1, 2 and 3) and by exposure status (PPC, PEC, PPI, and PEI). Limits of each box represent the first and the third quartile (25 and 75%) and the dots outside the boxes represent the outliers. The line dividing the box indicates the median value for each category. The null dotted line of each graph refers to the null median of each lesion calculated using all samples. Results of the statistical analysis, with significances, are reported in Table 1. (CP = CPD-64; Ox = 8oxoG; Al = AlkB; Ci = CisP; Ab = AbaS; Gl = glycol; Ct = CTRL.)

cellular aging. In parallel they observed a decrease of what they called the 8oxoG endonuclease activity (the repair activities that released 8oxodG from γ-ray-irradiated-DNA) as well as of the polymerase activities (DNA polymerases α, β and γ), as a function of cell population doublings [23]. Strikingly, the activities of polymerases α and β were hardly detected after 65 population doublings in fetal human fibroblasts. The experiments we present here were conducted with extracts prepared from cells gathered at passage 8, with an estimated number of population doubling around 40–50. Compared with our previous work that was performed with cells collected at passage 5 [17], the cells used for the present study have therefore undergone more doublings. Then, one should consider that *in vitro* aging could also contribute to the repair phenotypes that are observed in the present study. This could explain the lower excision/synthesis repair activities observed in the present study compared to our previous work, especially in the AG2 and AG3 groups that already exhibited repair activities decline at passage 5.

3.2. Apparent DNA repair on CTRL plasmid

In traditional excision/synthesis assays, the signal resulting from the control plasmid is usually subtracted from the signal obtained from the damaged plasmid [24–26]. We normally follow the same approach [12,19]. Accordingly, in the present study, the fluorescence that was incorporated into the undamaged CTRL plasmid was initially subtracted from the fluorescence incorporated into each damaged plasmid.

However, some samples from Age Groups 2 and 3 exhibited very low excision/synthesis repair capacity so that for certain lesions (among them 8oxoG, AlkB and AbaS) the resulting background-corrected signal was negative. This latter observation revealed that, for these samples only, more fluorescence was incorporated into the CTRL plasmid than the damaged plasmids. Thirty seven individuals out of 104 were concerned by this feature.

The strategy of subtracting the CTRL FI to lesion FI is valid when one postulates that the fluorescence resulting from the repair of lesions and the fluorescence incorporated in non-damaged plasmid (representing non specific background repair) are additive. Clearly in case of negative value, this is not the case.

All the slides and microarrays used to test the samples were extensively controlled and presented the same characteristics. We thus concluded that the low signals observed were specifically linked to the nature of the extracts. As it was a hallmark of samples from Age Group 2 and 3, we therefore hypothesized that it was related to some mechanisms specifically associated with aging.

The fluorescence incorporated into each plasmid is the endpoint of a multi-step process (recognition of the lesion, recruitment of excision proteins, synthesis of new DNA). In this study we used cells that had undergone numerous divisions during the *in vitro* culture. We know from the literature that aging is accompanied by a decline in the rate of DNA synthesis by polymerases in human and rodents [27] and that *in vitro* aging results in decrease in polymerase activities [23]. As part of a general decline of cell functions, the expression and/or activity of associated proteins important for

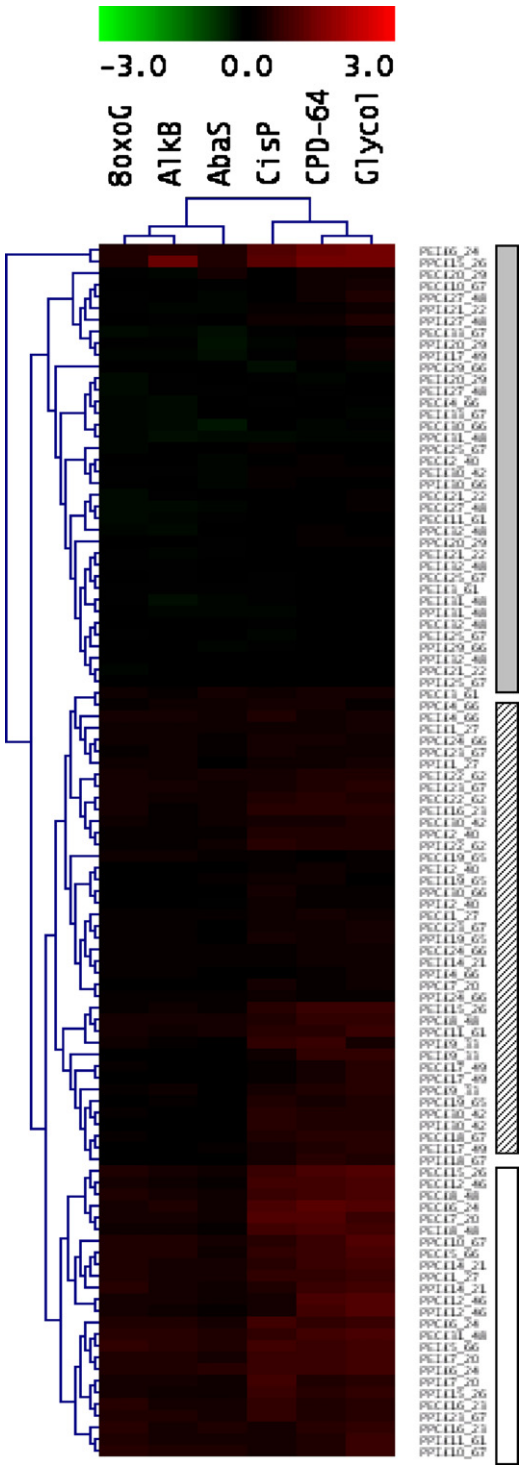

Fig. 3. Hierarchical clustering of all samples (Age Group 1, 2 and 3 for all exposure status) according to the repair of the 6 lesions (see Section 2 for details). The upper dendrogram represents the classification of the different lesions and thus of the corresponding repair pathways. 8oxoG, AlkB and AbaS, on the one hand, and CisP, CPD-64 and glycol, on the other hand, appeared in separated clusters. Each sample was represented by a line exhibiting its repair data for the 6 lesion families. The samples were divided in 3 clusters. First cluster (grey bar) comprised 8/36, 14/36 and 14/36 samples belonging to AG1, AG2 and AG3, respectively; second group (hatched bar) comprised 10/41 AG1, 10/41 AG2 and 21/41 AG3 samples; third group (white bar) comprised 13/25* AG1, 6/25 AG2 and 6/25 AG3 samples (*significant difference).

maintaining genomic integrity like helicases, nucleases or scaffolding proteins might also be deregulated in aging cells and affect DNA repair efficacy. This is dramatically illustrated by the premature aging phenotype associated with mutations in the WRN (Werner) protein, a protein of the RecQ helicase family that was found to be a partner of several BER proteins, including polymerase β [28].

We thus hypothesized that this inability of cell extracts to repair damaged plasmids as compared with non-damaged plasmid could reflect specific impairment of damage recognition or excision and/or of DNA synthesis; the rate-limiting activity of certain repair steps (opening of the helix by helicases) could for example become overwhelming in aging cells. Importantly, these features could be a "natural" feature of aging/*in vitro* aging. On the other hand, it has been demonstrated that mammalian cell free extracts can perform gratuitous repair on non-damaged DNA substrates [29]. We cannot exclude that in cells from elderly, the balance between gratuitous and specific repair is modified, resulting in more "non-specific" excision/synthesis reactions. These two hypotheses are not mutually exclusive. Because we cannot at that time determine the cause(s) of this higher fluorescence incorporation into the CTRL plasmid observed with some samples, we decided not to subtract the "background" and to analyze the CTRL fluorescence independently, as a *bona fide* repair activity.

3.3. Identification of DNA repair sub-pathways

3.3.1. PCA on standardized data

The first two components captured 94.15% of the variance within the dataset (Fig. 1). Within the limit of this plane, we observed from the correlation circle that 3 groups of repair pathways (variables) could be distinguished. The two main groups were constituted by 8oxoG, AlkB and AbaS on the one hand, and by CPD-64, CisP and glycol on the other hand. This observation allowed the ascription of the repair of these different groups of lesions to two distinct repair pathways. Obviously, repair of 8oxoG, AlkB and AbaS could be associated with BER. For the lesions of the second group, it can be that CPD-64, CisP and glycol were handled by a common repair pathway (nucleotide excision repair (NER is known to handle CPD-64 and CisP)) or, alternatively, by several identically regulated repair mechanisms (NER and an unspecified mechanism for glycol).

Interestingly, the isolated position of CTRL clearly indicated that it behaved differently from the "true" lesions, which was somehow expected. All these findings were globally confirmed by the Spearman correlation analysis (Supplemental data, Fig. B).

3.4. Determination of the influence of age and of UV-exposure on repair activities

To get a global view of the repair phenotypes according to both Age Group and exposure status, the data were allocated to their respective group. Each sample was characterized by 7 values (FI measured for the 6 lesions and for the CTRL). The set of all data are graphically represented as box-plots (Fig. 2) and, for clarity, significant differences between the different groups are reported in Table 1.

As can be seen on Fig. 2, analysis of the results according to exposure status revealed that all repair activities decline between Age Group 1 and Age Group 2, but this was significant only in the PPC group (Table 1). Similar results were found for TFI, corresponding to the cells excision/synthesis repair capacities, which significantly decreased between Age Group 1 and Age Group 2 and 3 (1 > 2 and 1 > 3), but only in what can be considered as the reference group (never exposed cells PPC; Supplemental data Fig. C). Strikingly, very few significant differences were found in the exposed groups: they concerned only repair of glycol and of CisP that significantly declined between Age Group 1 and 2 or 3, in PEC and PEI group (see

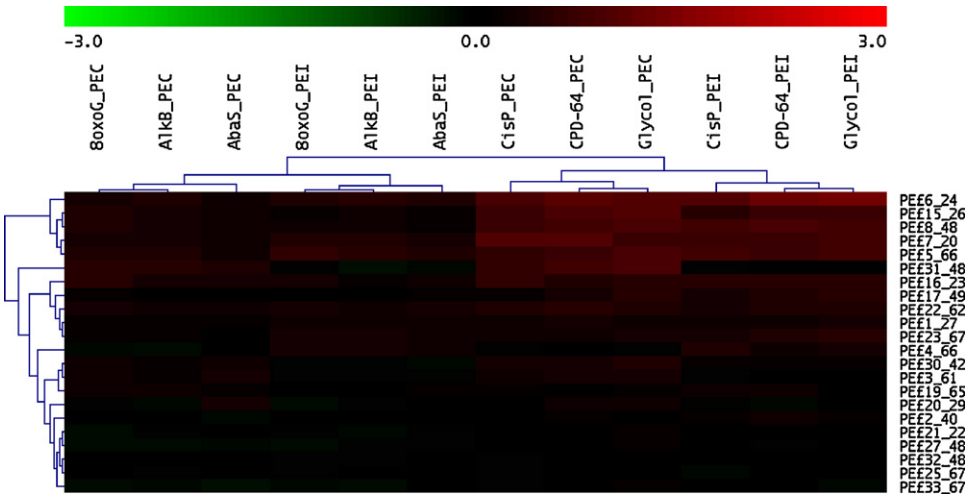

Fig. 4. Two-way ascending hierarchical classification performed on the PEC/PEI exposure couples. The upper dendrogram represents the classification of the different lesions with the associated exposure status. It can be noted that BER-associated lesions, on the one hand, and NER-associated lesions (including glycol), on the other hand, remained clustered independently of the exposure status. Further observation, however, clearly separated each repair group according to the exposure status emphasizing that the UVB-irradiation impacted globally on each repair group.

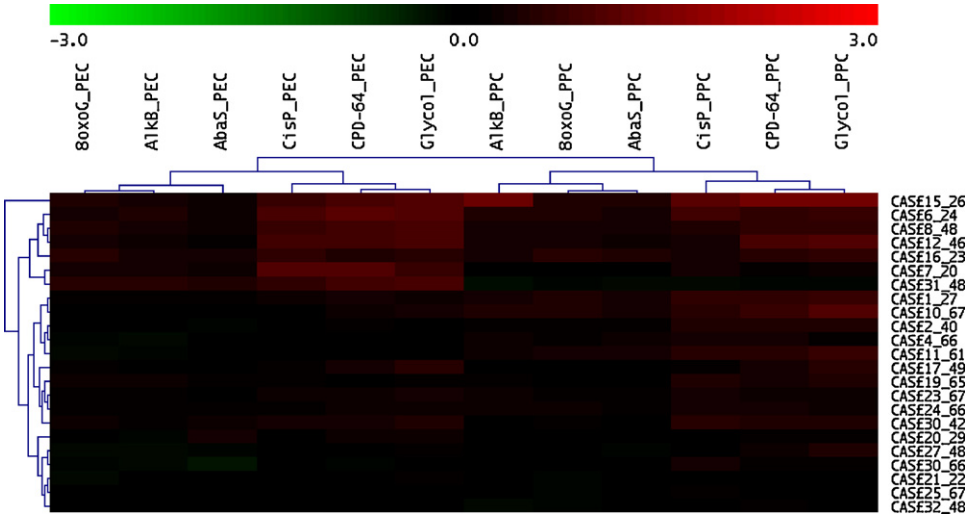

Fig. 5. Two-way ascending hierarchical classification performed on the PPC/PEC exposure couples. The upper dendrogram represents the classification of the different lesions with the associated exposure status. The clusters were separated according to the exposure status of the samples and subsequently separated by lesion group. In this latter case, the exposure status was the main factor that directed the classification underlying its strong impact globally on all repair pathways.

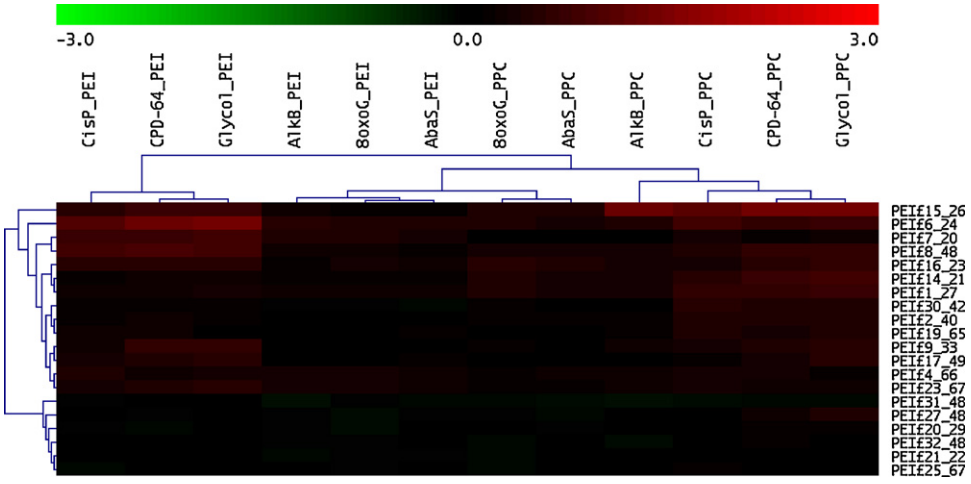

Fig. 6. Two-way ascending hierarchical classification performed on the PPC/PEI exposure couples. The upper dendrogram represents the classification of the different lesions with the associated exposure status. Three clusters could be distinguished here, separating the PEI NER-associated lesions (including glycol) from the other lesion groups. In addition, PEI-NER-associated lesions were markedly distant on the dendrogam which was the signature of a significant impact of the sun and UVB exposure on this specific repair pathway, as compared with PPC samples.

Table 2
Comparison of the variance of the fluorescence intensity (FIs) calculated for each Age Group (1, 2 and 3) and according to the exposure status of the samples, for each lesion.

Lesion type	1 > 2	1 > 3
CPD-64	PPI	PEC, PEI
8oxoG	PPI	
AlkB	PPI	
CisP	PPI	PEC
AbaS	PPI	
Glycol	PEI	PEI
CTRL	ND	ND

Only significant differences between Age Groups are reported (ND = non detected; $p < 0.05$ for all differences).

Table 1 for details). These latter findings were, at least partially, related to a more important dispersion of the data between groups as a consequence of sun- or UV-exposure, and consequently to a significantly enhanced variance. This was true for all lesions in PPI group between Age Group 1 and 2 (except for glycol) as well as for several lesions repaired by the NER-related pathway between Age Group 1 and 3 in PEC and PEI groups (Table 2). Substantial variation in DNA repair rates is generally observed between UV- or H_2O_2-treated human primary fibroblasts isolated from different individuals [11,30]. It seems reasonable to assume that the variance observed here illustrates the heterogeneity of the response induced in different individuals following sun photo-exposure and/or UV-irradiation. These variations might be linked not only to genetic heterogeneity and phototypes of the individuals but also to differences in their history of sun-exposure.

3.5. *Determination of the influence of chronic and acute photo-exposure*

The examination of the hierarchical clustering performed on the whole set of data clearly revealed two distinct groups of lesions (Fig. 3). One group was constituted by 8oxoG, AlkB and AbaS (called Group 8AA) and the other one included CisP, CPD-64 and glycol (called CCG). As in PCA, lesions repaired by BER and lesions repaired by NER were clearly dispatched in two groups and repair of glycol was associated with the NER group.

Examination of the hierarchical clustering performed on the exposure couples revealed interesting associations. For the couple PEC/PEI, the pattern depicted in the general hierarchical clustering was retained, i.e. the classification put group 8AA (of PEC and PEI) on one side, and group CCG (of PEC and PEI), on the other side. Importantly, within each lesion group, a clear separation between PEC and PEI was made (Fig. 4). Hence, in this case, the principal factor that directed the samples clustering was the lesion group type (either 8AA or CCG) and second factor was the exposure status. The same pattern of clustering was obtained for PPC/PPI, PEC/PPI and PEI/PPI, with some possible variation in the position of CisP (Supplemental data Fig. D). Importantly, in each case, the 8AA/CCG clustering differentiated the exposure groups.

In sharp contrast, in the analysis of the PPC/PEC pair, the main discriminating factor for clustering became the exposure status, revealing that chronic sun-exposure markedly affected all the repair pathways (Fig. 5). Interestingly, the PPC/PEI clustering was also guided by the exposure status but this time, the PPC CCG group and the PEI CCG group were pushed aside along the tree, showing that the combination of chronic sun exposure (E) and acute irradiation (I) specifically impacted the repair of the CCG lesion group, which includes CPD-64, i.e. characteristic UV-induced lesions handled by the NER pathway (Fig. 6). Hence, compared to the reference group PPC, PEC and PEI behave differently, indicating that chronic, lifelong exposure to sun light and acute UVB-irradiation elicit different responses. In addition, our results show that exposure of PE cells to a moderate UVB irradiation was characterized, after 24 h, by the induction of specific CCG-NER response.

Analysis of the samples axis showed, in most clusters, a tendency of the samples to be clustered by Age Group. However, it was not significant, except in few cases (Fig. 3 and Supplemental data Fig. D).

4. Conclusions

Our comprehensive approach showed that at least two differently regulated DNA repair pathways could be distinguished using our assay. We clearly demonstrated, from the photo-protected cell phenotypes, that excision/synthesis of all lesions decreased with aging, confirming that intrinsic aging is accompanied by a decline in DNA repair activities. In addition, the hierarchical clustering showed that (i) PEC was different from PPC, demonstrating that chronic sun-exposure induced changes in DNA repair activities, and (ii) a specific signature at the level of the NER pathway could be seen for the PEI/PPC cluster, indicating a direct effect of UVB irradiation on the repair pathway that takes in charge the main UVB-induced lesions, i.e. the photoproducts. Importantly, this UVB-irradiation induced signature was detected only using cells coming from chronically photo-exposed zones, revealing a cumulative effect of sun and UV exposure on the NER or NER-related pathway. Hence different environmental assaults specifically modulate distinct DNA repair pathways.

Effects of extrinsic/intrinsic aging on different repair pathways are certainly neither simple nor homogenous. We demonstrated here that the use of adapted bioinformatics tools is critical in deciphering the complexity of the data obtained with multiplexed functional DNA repair assay and unravelling the effects of environmental exposure on DNA repair.

Conflict of interest

There are no conflicts of interest.

Acknowledgements

We thank Dr. Serge Candéias for critical review of the manuscript. This study was partially funded by the CEA program “Technologies for Health” and by COMICS – FP6-2005 – LIFESCIHEALTH-7 – STREP – Contract No. 037575.

Appendix A. Supplementary data

Supplementary data associated with this article can be found, in the online version, at doi:10.1016/j.mrfmmm.2011.05.005.

References

[1] D.M. Wilson 3rd, V.A. Bohr, P.J. McKinnon, DNA damage, DNA repair, ageing and age-related disease, Mech. Ageing Dev. 129 (2008) 349–352.
[2] G.A. Garinis, G.T. van der Horst, J. Vijg, J.H. Hoeijmakers, DNA damage and ageing: new-age ideas for an age-old problem, Nat. Cell Biol. 10 (2008) 1241–1247.
[3] V. Gorbunova, A. Seluanov, Z. Mao, C. Hine, Changes in DNA repair during aging, Nucleic Acids Res. 35 (2007) 7466–7474.
[4] O.A. Sedelnikova, I. Horikawa, D.B. Zimonjic, N.C. Popescu, W.M. Bonner, J.C. Barrett, Senescing human cells and ageing mice accumulate DNA lesions with unrepairable double-strand breaks, Nat. Cell Biol. 6 (2004) 168–170.
[5] Y. Suh, J. Vijg, Maintaining genetic integrity in aging: a zero sum game, Antioxid. Redox Signal. 8 (2006) 559–571.
[6] B. Szczesny, K.K. Bhakat, S. Mitra, I. Boldogh, Age-dependent modulation of DNA repair enzymes by covalent modification and subcellular distribution, Mech. Ageing Dev. 125 (2004) 755–765.
[7] J.H. Chen, C.N. Hales, S.E. Ozanne, DNA damage, cellular senescence and organismal ageing: causal or correlative? Nucleic Acids Res. 35 (2007) 7417–7428.
[8] T Lu, T. Finkel, Free radicals and senescence, Exp. Cell Res. 314 (2008) 1918–1922.

[9] T. von Zglinicki, A. Burkle, T.B. Kirkwood, Stress, DNA damage and ageing – an integrative approach, Exp. Gerontol. 36 (2001) 1049–1062.
[10] D.L. Narayanan, R.N. Saladi, J.L. Fox, Ultraviolet radiation and skin cancer, Int. J. Dermatol. 49 (2010) 978–986.
[11] S. Sauvaigo, M. Bonnet-Duquennoy, F. Odin, F. Hazane-Puch, N. Lachmann, F. Bonté, R. Kurfürst, A. Favier, DNA repair capacities of cutaneous fibroblasts: effect of sun exposure, age and smoking on response to an acute oxidative stress, Br. J. Dermatol. 157 (2007) 26–32.
[12] B. Pons, A.S. Belmont, G. Masson-Genteuil, V. Chapuis, T. Oddos, S. Sauvaigo, Age-associated modifications of base excision repair activities in human skin fibroblast extracts, Mech. Ageing Dev. 131 (2010) 661–665.
[13] D.C. Cabelof, Aging and base excision repair: in need of a comprehensive approach, DNA Repair 6 (2007) 1399–1402.
[14] D. Goukassian, F. Gad, M. Yaar, M.S. Eller, U.S. Nehal, B.A. Gilchrest, Mechanisms and implications of the age-associated decrease in DNA repair capacity, FASEB J. 14 (2000) 1325–1334.
[15] S.Z. Imam, B. Karahalil, B.A. Hogue, N.C. Souza-Pinto, V.A. Bohr, Mitochondrial and nuclear DNA-repair capacity of various brain regions in mouse is altered in an age-dependent manner, Neurobiol. Aging 27 (2006) 1129–1136.
[16] S. Moriwaki, S. Ray, R.E. Tarone, K.H. Kraemer, L. Grossman, The effect of donor age on the processing of UV-damaged DNA by cultured human cells: reduced DNA repair capacity and increased DNA mutability, Mutat. Res. 364 (1996) 117–123.
[17] S. Sauvaigo, S. Caillat, F. Odin, A. Nkengne, C. Bertin, T. Oddos, Effect of aging on DNA excision/synthesis repair capacities of human skin fibroblasts, J. Invest. Dermatol. 130 (2010) 1739–1741.
[18] S. Moriwaki, Y. Takahashi, Photoaging and DNA repair, J. Dermatol. Sci. 50 (2008) 169–176.
[19] J.F. Millau, A.L. Raffin, S. Caillat, C. Claudet, G. Arras, N. Ugolin, T. Douki, J.L. Ravanat, J. Breton, T. Oddos, C. Dumontet, A. Sarasin, S. Chevillard, A. Favier, S. Sauvaigo, A microarray to measure repair of damaged plasmids by cell lysates, Lab. Chip 8 (2008) 1713–1722.
[20] R.D.C. Team, R: a language and environment for statistical computing, R foundation for statistical computing, Vienna, Austria, 2008, http://www.R-project.org.
[21] N.S. Holter, M. Mitra, A. Maritan, M. Cieplak, J.R. Banavar, N.V. Fedoroff, Fundamental patterns underlying gene expression profiles: simplicity from complexity, Proc. Natl. Acad. Sci. U.S.A. 97 (2000) 8409–8414.
[22] M.B. Eisen, P.T. Spellman, P.O. Brown, D. Botstein, Cluster analysis and display of genome-wide expression patterns, Proc. Natl. Acad. Sci. U.S.A. 95 (1998) 14863–14868.
[23] T. Kaneko, S. Tahara, T. Taguchi, H. Kondo, Accumulation of oxidative DNA damage, 8-oxo-2′-deoxyguanosine, and change of repair systems during in vitro cellular aging of cultured human skin fibroblasts, Mutat. Res. 487 (2001) 19–30.
[24] J.M. Barret, P. Calsou, B. Salles, Deficient nucleotide excision repair activity in protein extracts from normal human lymphocytes, Carcinogenesis 16 (1995) 1611–1616.
[25] L.J. Lipinski, N. Hoehr, S.J. Mazur, G.L. Dianov, S. Senturker, M. Dizdaroglu, V.A. Bohr, Repair of oxidative DNA base lesions induced by fluorescent light is defective in xeroderma pigmentosum group A cells, Nucleic Acids Res. 27 (1999) 3153–3158.
[26] R.D. Wood, P. Robins, T. Lindahl, Complementation of the xeroderma pigmentosum DNA repair defect in cell-free extracts, Cell 53 (1988) 97–106.
[27] D. Srivastava, D.L. Busbee, Replicative enzymes, DNA polymerase alpha (pol alpha), and in vitro ageing, Exp. Gerontol. 38 (2003) 1285–1297.
[28] V.A. Bohr, Rising from the RecQ-age: the role of human RecQ helicases in genome maintenance, Trends Biochem. Sci. 33 (2008) 609–620.
[29] M.E. Branum, J.T. Reardon, A. Sancar, DNA repair excision nuclease attacks undamaged DNA. A potential source of spontaneous mutations, J. Biol. Chem. 276 (2001) 25421–25426.
[30] M. Chazal, E. Roux, C. Alapetite, C. Roulin, E. Moustacchi, T. Douki, C. Baudouin, M. Charveron, N. Basset-Seguin, Interexperimental and interindividual variations of DNA repair capacities after UV-B and UV-C irradiations of human keratinocytes and fibroblasts, Photochem. Photobiol. 79 (2004) 286–290.